

Polaron formation in the optimally doped ferromagnetic manganites $\text{La}_{0.7}\text{Sr}_{0.3}\text{MnO}_3$ and $\text{La}_{0.7}\text{Ba}_{0.3}\text{MnO}_3$

Y. Chen

*NIST Center for Neutron Research, National Institute of Standards and Technology, Gaithersburg, MD 20899 and
Dept. of Materials Science and Engineering, University of Maryland, College Park, MD 20742*

B. G. Ueland and J. W. Lynn

NIST Center for Neutron Research, National Institute of Standards and Technology, Gaithersburg, MD 20899

G. L. Bychkov and S. N. Barilo

Institute of Solid State and Semiconductor Physics, Academy of Science, Minsk 220072, Belarus

Y. M. Mukovskii

Moscow State Steel and Alloys Institute, Moscow 119049, Russia

(Dated: April 13, 2021)

The nature of the polarons in the optimally doped colossal magnetoresistive (CMR) materials $\text{La}_{0.7}\text{Ba}_{0.3}\text{MnO}_3$ (LBMO) and $\text{La}_{0.7}\text{Sr}_{0.3}\text{MnO}_3$ (LSMO) is studied by elastic and inelastic neutron scattering. In both materials, dynamic nanoscale polaron correlations develop abruptly in the ferromagnetic state. However, the polarons are not able to lock-in to the lattice and order, in contrast to the behavior of $\text{La}_{0.7}\text{Ca}_{0.3}\text{MnO}_3$. Therefore ferromagnetic order in LBMO and LSMO survives their formation, explaining the conventional second order nature of the ferromagnetic-paramagnetic transition. Nevertheless, the results demonstrate that the fundamental mechanism of polaron formation is a universal feature of these ferromagnetic perovskite manganites.

PACS numbers: 75.47.Gk, 71.38.-k, 63.20.kd, 61.05.F-

I. INTRODUCTION

The discovery of colossal magnetoresistance (CMR) in the hole-doped perovskite manganites of the form $\text{La}_{1-x}\text{A}_x\text{MnO}_3$ (A=Ca, Ba and Sr) has generated much interest^{1,2}. The parent compound LaMnO_3 is an antiferromagnetic insulator, with a Mn-O sublattice consisting of a network of corner-sharing Mn^{3+}O_6 octahedra. The Mn^{3+} ion has three t_{2g} electrons that form its $S=3/2$ core-spin and one additional electron in its higher energy, doubly-degenerate e_g orbital. The Jahn-Teller distortion of the MnO_6 octahedron removes the degeneracy of the e_g levels and the ground state consists of an ordered array of distorted octahedra with antiferromagnetic order of the Mn spins. With substitution of trivalent La^{3+} by divalent alkaline-earth metal ions such as Ca^{2+} , Ba^{2+} , or Sr^{2+} , holes are introduced into the material, producing Mn^{4+} ions where the e_g orbital is unoccupied. With sufficient hole doping (typically $0.2 < x < 0.5$) the ground state becomes a magnetically isotropic ferromagnetic metal. In this regime the basic relationship between conductivity and ferromagnetism has been understood by the double-exchange (DE) mechanism³, in which itinerant e_g electrons associated with the Mn^{3+} hop between the localized Mn^{4+} ions, providing both ferromagnetic exchange (due to the strong Hund's rule coupling between the t_{2g} and e_g electrons) and electrical conduction. The DE interaction competes with a strong electron-phonon coupling via the Jahn-Teller active Mn^{3+} ions. The hopping of an electron, with its associated lattice distortion, forms a polaron. Here we focus on the regime near optimal doping

for ferromagnetism, where CMR is observed. At optimal doping, this competition produces a transition from the ferromagnetic-metallic ground state to an intrinsically inhomogeneous paramagnetic-insulating state at elevated temperatures, which is often described as polaronic^{4,5}.

For the prototype $\text{La}_{0.7}\text{Ca}_{0.3}\text{MnO}_3$ (LCMO) system the ferromagnetic state has been found to be truncated by the formation of static nanoscale lattice polarons,^{6,7,8,9,10} driving the ferromagnetic-paramagnetic transition first-order^{6,11,12,13,14,15,16}. These polarons^{17,18} make the system especially sensitive to applied magnetic fields, amplifying the magnetoresistivity near T_C . In LCMO, polaron correlations develop within a narrow temperature regime as T_C is approached from low temperatures, with a nanoscale correlation length that is only weakly temperature dependent. Polarons take the form of CE-type correlations with an ordering wave vector of $\approx (1/4, 1/4, 0)$ (with respect to the cubic perovskite cell). The static nature of these short range polaron correlations indicates the presence of a glass-like state^{6,7,12}. In addition, dynamic correlations exist with a comparable correlation length and with an energy distribution that is quasielastic. The elastic polaron scattering disappears at higher temperature, above which the correlations are purely dynamic¹⁵. While these CE correlations characterize the insulating state above T_C , the onset of ferromagnetism leads to their melting.

In the closely related $\text{La}_{0.7}\text{Ba}_{0.3}\text{MnO}_3$ (LBMO)^{19,20} and $\text{La}_{0.7}\text{Sr}_{0.3}\text{MnO}_3$ (LSMO)^{21,22} ferromagnets, on the other hand, the ferromagnetic transition is a conventional

second-order one, and no polaron order is observed. In the present work we have found that nanoscale polarons do indeed form in optimally doped LSMO and LBMO, well below T_C , in the ferromagnetic state. However, these polarons are purely dynamic in nature, and never lock-in to the lattice to form an ordered state. The ferromagnetic state therefore survives their formation, and a conventional second-order transition is realized at higher temperatures, well above the temperature where the polarons form. The present results demonstrate that intrinsic inhomogeneities on a nanometer length scale are a universal feature of these ferromagnetic manganites, while the ferromagnetic state is only terminated if the polarons condense to form a (static) glass phase.^{15,23}

II. EXPERIMENTAL PROCEDURES

Elastic and inelastic neutron scattering measurements were carried out to study the polaron correlations in single crystals of $\text{La}_{0.7}\text{Sr}_{0.3}\text{MnO}_3$ and $\text{La}_{0.7}\text{Ba}_{0.3}\text{MnO}_3$ weighing approximately 3 and 1 grams, respectively. These crystals have second-order ferromagnetic transitions as evidenced by the temperature dependence of the magnetic Bragg peaks as well as the small wave vector spin wave dispersion data, and are the same crystals used in earlier studies, with T_C 's of 351 K²² and 336 K,¹⁹ respectively. The neutron data were obtained on the BT-7 and BT-9 thermal triple axis spectrometers at the NIST Center for Neutron Research. We used pyrolytic graphite (PG) (002) monochromators and PG (002) analyzers. PG filters of 5 cm thickness were used to eliminate higher-order contamination. For BT-7 measurements, horizontal collimators with divergences of 100', 50', 50' and 100' full width at half maximum (FWHM) were used before and after the monochromator, after the sample, and before the detector, respectively. For BT-9 measurements, collimations were 40'-47'-40'-80'. Samples were sealed in an aluminum can containing helium exchange gas and mounted in a closed cycle refrigerator operating over a temperature range from 10 K to 400 K. The crystal structure of LSMO and LBMO is orthorhombic, but only slightly distorted from the cubic lattice, and since the crystals are twinned for simplicity we label wave vectors in the reciprocal lattice units appropriate for pseudocubic unit cells with lattice parameters of $a = 3.8660 \text{ \AA}$ and $a = 3.9232 \text{ \AA}$ (at 360 K) for LSMO and LBMO, respectively. In this notation the polaron correlations are observed around $(1/4, 1/4, 0)$ and equivalent positions (CE-type lattice correlations), in reciprocal lattice units (rlu) defined by $a^* = 2\pi/a$.

III. EXPERIMENTAL RESULTS

Figure 1 shows a color map of the neutron intensity above T_C for each system as a function of (\mathbf{Q}, E) . We see that the dynamic correlations are observed and are

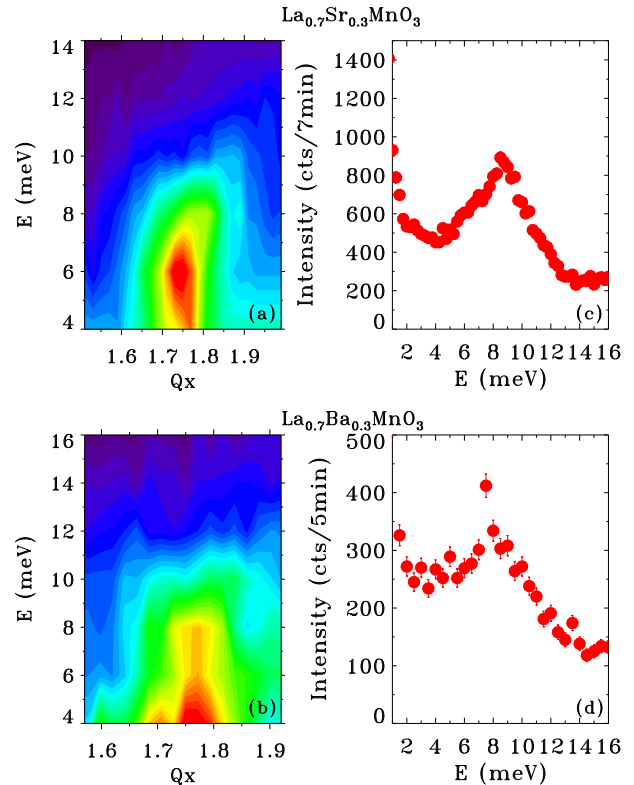


FIG. 1: (color online) (\mathbf{Q}, E) map of inelastic neutron scattering intensity around $\mathbf{Q} = (1.5+q, 2+q, 0)$ (cubic notation) at $T = 360 \text{ K}$ for (a) LSMO and (b) LBMO. Dynamic polaron scattering is observed around the $q = (1/4, 1/4, 0)$ reduced wave vector position. (c) and (d) show an energy scan at $\mathbf{Q} = (1.75, 2.25, 0)$ for LSMO and LBMO, respectively, at $T = 360 \text{ K}$, revealing that the scattering has a broad maximum at finite energy, in addition to a quasielastic component. The energy resolution at the elastic position is 1.5 meV. Error bars where shown are statistical in nature and represent one standard deviation.

peaked around the $\mathbf{Q} = (1.75, 2.25, 0)$ position, as expected for these CE-type lattice correlations. The intensity for LSMO has a broad maximum in energy, which can be seen more clearly in the energy scan shown in Fig. 1(c). For LBMO this maximum occurs at a somewhat lower energy (Fig. 1(d)). These data were taken with the same instrumental conditions, and recalling that the LSMO sample is $3\times$ larger than the LBMO sample, we see that the strength of the polaron scattering is comparable in the two systems. The scattering extends to low energies, and appears to consist of two components, a quasielastic component (a Lorentzian centered at $E=0$) and a component that has a broad maximum at finite energy. At higher energies the scattering decreases

fairly rapidly. The overall behavior is quite similar to the dynamics observed in LCMO¹⁵, where again there is a quasielastic component to the scattering along with a component that peaks at finite energy. In that case it was difficult to extract a quasielastic linewidth vs. temperature, in contrast to what was done for the lower T_C bilayer system.²³ This is because of the difficulty in establishing ‘background’ at these elevated temperatures, as well as the difficulty in separating the (apparent) two components of the scattering. In the present case the T_C ’s are even higher than for LCMO, and hence it is even more difficult to extract detailed quasielastic linewidths as a function of T . The general behavior, on the other hand, is clear.

To investigate the temperature dependence of the dynamic polaron correlations, \mathbf{Q} scans around the $(1/4,1/4,0)$ position were carried out for a series of energy transfers over a wide temperature range. The dynamic polaron scattering is very broad in energy, and broader than the instrumental resolution in \mathbf{Q} as well. Hence, it is generally better to use \mathbf{Q} -scans to measure the scattering since the scattering is confined to a relatively small range and the resolution does not vary over the scan. Both the \mathbf{Q} -width and energy width of the measured peaks are not resolution limited, and \mathbf{Q} -scans can be performed in a wide energy range to observe the dynamic polaron correlations. Fig. 2 shows data as a function of $\mathbf{Q} = (1.5-q, 1.5+q, 0)$ for LSMO. To search for static CE-type polaron correlations, extensive elastic scans ($E = 0$) were performed above and below T_C . No evidence of ordered polarons was observed at any temperature, as indicated in the data shown in Fig. 2(a). This contrasts with the behavior of LCMO, where short-range static CE-type polaron correlations abruptly develop at T_C ,^{6,7} and truncate the ferromagnetic state.^{12,15}

The inelastic scattering, on the other hand, conveys a completely different story. At $T = 100$ K and 200 K there is no evidence in LSMO of any peak in the scattering, with featureless scattering that is weakly temperature dependent and likely originates from multiphonon and multimagnon (background) scattering. At 240 K, however, a distinct peak centered at $\mathbf{Q} \approx (1.75, 2.25, 0)$ abruptly appears. Note that this temperature is far below T_C . The wave-vector width of this peak is approximately temperature and energy independent and corresponds to a correlation length of ≈ 1 nm (10 \AA). Similar behavior is observed for LBMO, where Fig. 2(c) shows \mathbf{Q} scans measured at an energy transfer of $E = 8$ meV between $T = 100$ K and 390 K. A peak in the scattering is observed at and above 150 K, while no peak is observed at lower T . Hence in both systems we observe the abrupt development of short-range dynamic polaron correlations well below T_C , which evolve through T_C without any apparent indication that long range ferromagnetic order has been lost. These dynamic correlations persist up to high temperatures, likely all the way up to the orthorhombic-rhombohedral transition.^{9,18}

The data in Fig. 2 have been fit to a linear background

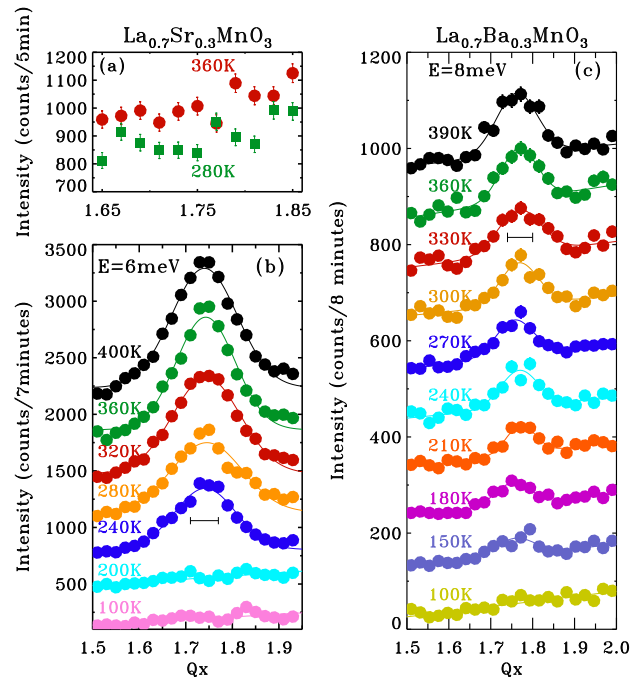


FIG. 2: (color online) (a) Elastic scan through the polaron position for LSMO above and below T_C . No static polaron peaks were observed at any of the $(1/4,1/4,0)$ positions for either LSMO or LBMO. (b) Temperature dependence of the inelastic scattering for LSMO at an energy transfer of $E = 6$ meV for $\mathbf{Q} = (1.5+q, 2+q, 0)$. The scattering at successive temperatures has been displaced vertically by 280 counts for clarity. A peak in the scattering abruptly appears around $T = 240$ K, and persists to higher temperatures. The horizontal bar indicates the q -resolution (FWHM). (c) Temperature dependence of the inelastic scattering in LBMO at an energy transfer of $E = 6$ meV for $\mathbf{Q} = (1.5+q, 2-q, 0)$. The scattering at successive temperatures has been displaced vertically by 100 counts for clarity. A peak in the scattering abruptly appears around $T = 150$ K, and persists up to high temperature. The horizontal bar indicates the q -resolution (FWHM).

plus a Gaussian peak. Once the peak appears, its observed intensity increases with increasing T and follows the thermal occupancy factor for a boson excitation. The results for the integrated intensities, after correcting for the Bose thermal factor, are shown in Fig. 3. Fig. 3(a, c) shows that the inelastic scattering abruptly appears at a well defined temperature, and then is constant in strength. Therefore this overall scattering behaves as a phonon excitation. The width of the scattering (Fig.

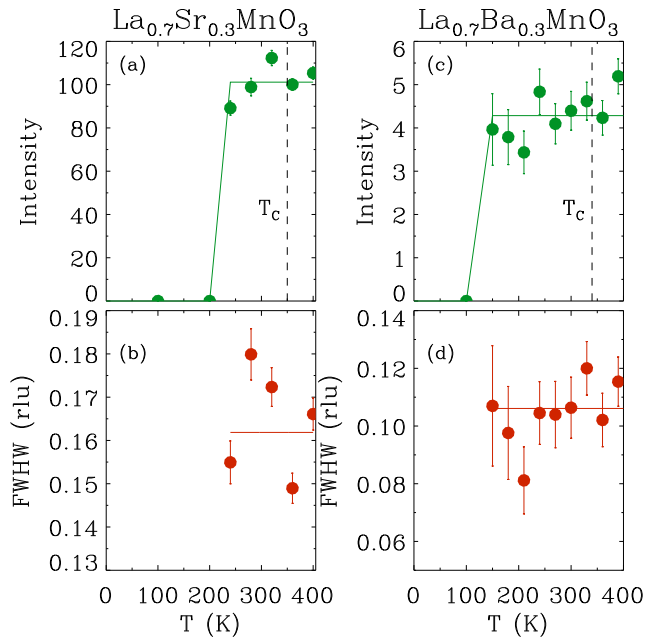


FIG. 3: (color online) [(a) and (c)] Temperature dependence of the inelastic scattering intensity shown in Fig. 2 (a) for LSMO and (c) LBMO. The integrated intensity of the scattering abruptly appears at a temperature well below T_C , and then is constant at higher temperature after the Bose-Einstein thermal population factor has been divided out. (b,d) Temperature dependence of the intrinsic width in Fig. 2 for (b) LSMO and (d) LBMO. The width is found to be temperature independent. Neither the width nor the intensity are sensitive to the ferromagnetic ordering.

3(b,d)), once the intensity appears, is also independent of temperature. Hence the correlation length in real space remains at $\approx 1nm$ throughout the entire temperature range where this scattering is observed.

IV. DISCUSSION AND CONCLUSIONS

The development of static CE-type correlations has been shown to have important implications for the ferromagnetic to paramagnetic transition in the CMR manganites. When static polarons form in LCMO, electrons become trapped, driving the system into an insulating state (hopping conductivity). The transition into the insulating state is accompanied by a trun-

	Ca	Sr	Ba
$a(\text{\AA})$	3.868	3.866	3.923
$T_C(K)$	257	351	336
$\xi(\text{\AA})$	11.1(3)	7.7(3)	11.3(3)

TABLE I: Comparison of the lattice parameters, ferromagnetic transition temperatures, and size of the polarons for LCMO, LBMO, and LSMO.

cation of the ferromagnetic state in a discontinuous fashion¹². Above T_C , the nature of the order is a polaron glass, in that the correlations are short range, and static.^{15,23} The short range correlations make the system especially sensitive to modest magnetic fields that can then drive the paramagnetic-insulating-ferromagnetic-metallic transition, with the concomitant large change in electrical conductivity^{17,18}. At sufficiently high T the glass order disappears while dynamic polaron correlations persist as a polaron liquid. In LCMO, we observed a sharp phonon at 8 meV in the ferromagnetic metallic state below T_C ¹⁵. Above T_C , the phonon is still present, and interacts with the dynamic polarons. However, no such phonon is observed in this energy range in LSMO and LBMO. Hence, the observed scattering is purely from the polaron correlations.

In the course of the initial studies on LCMO,⁶ a search for these polarons peaks was made in LBMO and LSMO, but no static polaron correlations were found. Indeed for the latter materials the ferromagnetic transition is a conventional second order one, with properties like the magnetization and spin wave stiffness quantitatively exhibiting scaling behavior,^{19,20,21,22} while the rather large changes in the resistivity can be understood on the basis of conventional electron scattering by magnetic fluctuations.²⁴ The behavior of the resistivity is also different than for LCMO, which peaks at T_C when the polarons develop. For LSMO $\rho(T)$ increases with T (i.e. is metallic-like) both below and above T_C ,²⁵ while for LBMO $\rho(T)$ peaks, but only well above T_C .¹⁹ The polarons in LBMO and LSMO abruptly develop, but well below T_C , and there is no obvious effect on the resistivity. The sizes of the polarons in all three systems are very similar as shown in Table 1, where the size has been taken from the width of the inelastic scattering. We note that the strength of the scattering, which is related to the number of polarons (since the size is temperature independent), is also comparable in the three systems. Hence it is not clear why only the polarons in LCMO lock-in to the lattice and truncate the ferromagnetic state, even though the polarons in LBMO and LSMO form at lower temperature (particularly in comparison to T_C) but never lock-in. It is also not clear what is controlling the temperature of formation of the polarons, either static or dynamic, in these ferromagnetic metallic systems. We hope that the present studies will stimulate theoretical studies to address these issues.

ACKNOWLEDGMENTS

We thank Elbio Dagotto, Dimitri Argyriou, and Adriana Moreo for stimulating discussions. Work in Belarus

was supported in part by BRFFI, Grant No. F-08R-177.

-
- ¹ E. Dagotto, *Nanoscale Phase Separation and Colossal Magnetoresistance: The Physics of Manganites and Related Compounds* (Springer-Verlag, New York, 2002).
- ² Y. Tokura, Rep. Prog. Phys. **69**, 797 (2006).
- ³ C. Zener, Phys. Rev **82**, 403 (1951).
- ⁴ A. J. Millis, P. B. Littlewood, B. I. Shraiman, Phys. Rev. Lett. **74**, 5144 (1995).
- ⁵ A. J. Millis, Phys. Rev. B **53**, 8434 (1996).
- ⁶ C. P. Adams, J. W. Lynn, Y. M. Mukovskii, A. A. Arsenov, and D. A. Shulyatev, Phys. Rev. Lett **85**, 3954 (2000).
- ⁷ P. Dai, J. A. Fernandez-Baca, N. Wakabayashi, E. W. Plummer, Y. Tomioka, and Y. Tokura, Phys. Rev. Lett. **85**, 2553 (2000).
- ⁸ C. S. Nelson, M. v. Zimmermann, Y. J. Kim, J. P. Hill, D. Gibbs, V. Kiryukhin, T. Y. Koo, S.-W. Cheong, D. Casa, B. Keimer, et al., Phys. Rev. B **64**, 174405 (2001).
- ⁹ V. Kiryukhin, A. Borissov, J. S. Ahn, Q. Huang, J. W. Lynn, and S.-W. Cheong, Phys. Rev. B **70**, 214424 (2004).
- ¹⁰ J. W. Lynn, C. P. Adams, Y. M. Mukovskii, A. A. Arsenov, and D. A. Shulyatev, J. Appl. Phys. **89**, 6846 (2001).
- ¹¹ J. W. Lynn, R. W. Erwin, J. A. Borchers, Q. Huang, A. Santoro, J.-L. Peng, and Z. Y. Li, Phys. Rev. Lett. **76**, 4046 (1996).
- ¹² C. P. Adams, J. W. Lynn, V. N. Smolyaninova, A. Biswas, R. L. Greene, W. Ratcliff, S.-W. Cheong, Y. M. Mukovskii, and D. A. Shulyatev, Phys. Rev. B **70**, 134414 (2004).
- ¹³ D. Kim, B. Revaz, B. L. Zink, F. Hellman, J. J. Rhyne, and J. F. Mitchell, Phys. Rev. Lett. **89**, 227202 (2002).
- ¹⁴ F. Rivadulla, M. Otero-Leal, A. Espinosa, A. de Andrés, C. Ramos, J. Rivas, and J. B. Goodenough, Phys. Rev. Lett. **96**, 016402 (2006).
- ¹⁵ J. W. Lynn, D. N. Argyriou, Y. Ren, Y. Chen, Y. M. Mukovskii, and D. A. Shulyatev, Phys. Rev. B **76**, 014437 (2007).
- ¹⁶ L. Demko, I. Kezsmarki, G. Mihaly, N. Takeshita, Y. Tomioka, and Y. Tokura, Phys. Rev. Lett. **101**, 037206 (2008).
- ¹⁷ L. Downward, F. Bridges, S. Bushart, J. J. Neumeier, N. Dilley, and L. Zhou, Phys. Rev. Lett. **95**, 106401 (2005).
- ¹⁸ J. A. Souza, J. J. Neumeier, and Y.-K. Yu, Phys. Rev. B **78**, 014436 (2008).
- ¹⁹ S. N. Barilo, G. L. Bychkov, L. A. Kurnevich, S. V. Shiryaev, L. A. Kurochkin, J. W. Lynn, and L. Vasiliu-Doloc, J. Cryst. Growth **211**, 480 (2000).
- ²⁰ W. Jiang, X. Z. Zhou, , G. Williams, Y. Mukovskii, and K. Glazyrin, Phys. Rev. B **77**, 064424 (2008).
- ²¹ K. Ghosh, C. J. Lobb, R. L. Greene, S. G. Karabashev, D. A. Shulyatev, A. A. Arsenov, and Y. Mukovskii, Phys. Rev. Lett. **81**, 4740 (1998).
- ²² L. Vasiliu-Doloc, J. W. Lynn, A. A. A. Y. M. Mukovskii, and D. A. Shulyatev, J. Appl. Phys. **83**, 7342 (1998).
- ²³ D. N. Argyriou, J. W. Lynn, R. Osborn, B. Campbell, J. F. Mitchell, U. Ruett, H. N. Bordallo, A. Wildes, and C. D. Ling, Phys. Rev. Lett. **89**, 036401 (2002).
- ²⁴ M. E. Fisher and J. S. Langer, Phys. Rev. Lett. **20**, 665 (1968).
- ²⁵ A. Urushibara, Y. Moritomo, T. Arima, A. Asamitsu, G. Kido, and Y. Tokura, Phys. Rev. B **51**, 14103 (1995).